

Adsorption material composition and process optimization, a systematical approach based on Deep Learning

Maria João Regufe^{a*}, Vinícius V. Santana^b, Márcio M. Martins^b, Alexandre F. P. Ferreira^a, José M. Loureiro^a, Alírio E. Rodrigues^a, Ana M. Ribeiro^a, Idelfonso B. R. Nogueira^{a*}

^aLaboratory of Separation and Reaction Engineering, Associate Laboratory LSRE-LCM
Department of Chemical Engineering, Faculty of Engineering, University of Porto
Rua Dr. Roberto Frias, 4200-465, Porto, Portugal.

^bDepartamento de Engenharia Química, Escola Politécnica (Polytechnic School),
Universidade Federal da Bahia, R. Prof. Aristides Novis, 2 - Federação, 40210-630, Salvador - BA, Brazil.

*(e-mail: mjregufe@fe.up.pt; idelfonso@fe.up.pt)

Abstract: The material screening is a preliminary step while designing an adsorption process. This step is carried out with a limited view of what concerns the material used. It usually focuses only on the materials' properties and not on their behavior while employed in the separation process. Furthermore, there is a lack of a systematic approach that uses an available materials database to identify the best material in a given process application. This leaves an open issue in the literature, which is getting attention with the advance of computer sciences. Hence, this work addresses this topic by proposing a systematic approach based on Deep Learning and a meta-heuristic optimization for simultaneous adsorbent screening and process optimization. This approach is developed with the main goal to make available a methodology for process optimization with material design that can be run at any time that the process needs to be reconfigured, without exhaustive simulations. As a case study, it is presented the carbon dioxide capture by Electric Swing Adsorption. The results show that the proposed methodology can identify the optimal material composition while providing the optimal process operating conditions.

Keywords: Adsorbents screening; Deep Learning; CO₂ capture; Electric Swing Adsorption; Multi-level Optimization.

1. INTRODUCTION

It is possible to note a rising interest in the literature to apply Artificial Intelligence to address material science problems. As presented by Ongari, Talirz, and Smit (2020), the recent growth of computational power allows the use of the continually growing material properties database towards matching the ideal available material to the application. However, it is still necessary to reach further developments that allow this bridge between computer and material sciences. Another point of view of this problem is how the ideal material is the optimal option? In Rajagopalan, Avila, and Rajendran (2016), the authors raised a similar question, which is the title of their work "Do adsorbent screening metrics predict process performance?". Usually, in the material science literature, a given adsorbent's performance is evaluated separately from its industrial application. Therefore, a material that presents right adsorption metrics in adsorbent screening might not be the option that will lead to the application scenario's optimal operation. However, the simultaneous processes optimization and adsorbent screening might be an exhaustive task, mainly due to the heavy computation cost associated with cyclic adsorption models. This effort can be overtaken using artificial intelligence techniques, especially the Deep Neural Networks (DNN). The application of DNN to address dynamic problems in chemical engineering is a recent field. In Oliveira et al. (2020), the authors propose for the first time the application of

DNN models to address the cyclic adsorption modeling. In the referred work, the authors demonstrated that the DNN models can represent the process dynamics with more fidelity than other machine learning approaches, such as shallow recurrent neural networks and the feed-forward ones. Following those conclusions and extending the DNN's field of application in chemical engineering, this work proposes identifying a DNN model to address the simultaneous process optimization and materials screening. The main benefit of using the DNN approach for this case is its low computation cost, when comparing to the usage of phenomenological models. For instance, the execution time for an Artificial Intelligence model can be some seconds while a cyclic adsorption first principle model might require several minutes up to hours to reach a cyclic steady state (Wang et al., 2003; Nogueira et al., 2017, 2018; Oliveira et al., 2020).

Therefore, this work proposes a systematic optimization procedure in order to simultaneously define a process optimal operating condition and the optimal option of adsorbent among a known and available set of materials. The methodology is idealized for cases where it is necessary a process reconfiguration during an operating campaign. Therefore, requiring a solution that can be quickly available, which would not be possible using first-principles models. As a study case, the optimization of an Electrical Swing Adsorption (ESA) unit operation for CO₂ capture is presented. The ESA is a cyclic adsorption process in which the heat is generated by Joule

effect. It is claimed that this process has the potential to promote CO₂ capture efficiently. In Regufe et al. (2020) is reported an extensive study of hybrid materials composed of zeolite 13X (having good CO₂ adsorption capacity properties) and activated carbon (having good electric properties) in different compositions: only activated carbon (100%AC), with 70% of activated carbon and 30% of zeolite 13 X (70%AC-30%13X) and 50%/50% of zeolite 13X/activated carbon, respectively. These materials were shaped into pellets by extrusion. Thus, the materials presented in the referred work will be here used as decision variables in the proposed optimization problem. Hence, it is possible to perform a systematic materials screen together with the unit operation optimization.

The methodology here proposed can be schematically represented in three steps as:

- Definition of decision variables and optimization goals;
- Empirical model identification;
- Optimization problem definition.

2. DEFINITION OF DECISION VARIABLES AND OPTIMIZATION GOALS

A rigorous mathematical model of the ESA process was used as a virtual plant to generate the database for the empirical model identification. The model was validated experimentally by Regufe et al. (2020). This model contains the mass, energy, and momentum balances to describe multicomponent adsorption dynamic behaviour in a fixed-bed. The following assumptions were considered:

- ideal gas behaviour for the gas phase;
- constant porosity along the bed;
- no mass, heat or velocity gradients in the radial dimension;
- internal mass transfer resistance described by the Linear Driving Force (LDF) model;
- absence of temperature gradients within the solid particle, since the heat transfer in the solid is much faster than in the gas phase;
- axially dispersed plug flow;
- the Ergun equation is valid locally, i.e., in the momentum balance, only the terms of pressure drop and velocity change are considered.

The model is composed by the following equations.

Material balance in the gas phase:

$$\frac{\partial}{\partial z} \left(\varepsilon_b D_{ax} C_{gt} \frac{\partial y_i}{\partial z} \right) - \frac{\partial}{\partial z} (u_0 C_{gi}) - \varepsilon_b \frac{\partial C_{gi}}{\partial t} - (1 - \varepsilon_b) a_p k_f (C_{gi} - C_{si}) = 0 \quad (1)$$

where z is the axial position, t is the time, ε_b is the bed porosity, u_0 is the superficial velocity, C_{gt} and C_{gi} are respectively the total and component i gas-phase concentrations, y_i is the molar fraction of component i , C_{si} is the concentration of component i at the gas-solid interface, D_{ax} is the mass axial dispersion coefficient, k_f is the film mass transfer coefficient, a_p is the particle external specific area.

Momentum balance (Ergun equation):

$$-\frac{\partial P}{\partial z} = \frac{150 \mu_g (1 - \varepsilon_b)^2}{\varepsilon_b^3 d_p^2} u_0 + \frac{1.75 (1 - \varepsilon_b) \rho_g}{\varepsilon_b^3 d_p} |u_0| u_0 \quad (2)$$

where P is the total pressure, μ_g is the gas viscosity, ρ_g is the gas density and d_p is the particle diameter.

The particles porosity was considered to be bidisperse, containing macropores and crystals, and the mass transfer resistance was modeled in each using the linear driving force models in series (bi-LDF):

$$\frac{\partial \bar{C}_i}{\partial t} = \frac{15 D_{pi}}{R_p^2} (C_{si} - \bar{C}_i) - \frac{\rho_p}{\varepsilon_p} \frac{\partial \bar{q}_i}{\partial t} \quad (3)$$

where D_{pi} is the pore diffusivity of component i , R_p is the particle radius, ρ_p is the particle density, ε_p is the particle porosity, \bar{C}_i is the average concentration in the mesopores/macropores of component i , and \bar{q}_i is the average adsorbed phase concentration of component i .

Mass balance in the micropores, also described by the Linear Driving Force model:

$$\frac{\partial \bar{q}_i}{\partial t} = \frac{15 D_{ci}}{R_c^2} (q_i^* - \bar{q}_i) \quad (4)$$

where D_{ci} is the crystal diffusivity, R_c is the crystal radius, q_i^* is the adsorbed phase concentration of component i in equilibrium with \bar{C}_i calculated with the multicomponent Dual-Site Langmuir isotherm model.

The fluxes equality at the particle surface:

$$\frac{a_p k_f}{\varepsilon_p} (C_{gi} - C_{si}) = \frac{15 D_{pi}}{R_p^2} (C_{si} - \bar{C}_i) \quad (5)$$

The gas phase energy balance:

$$\frac{\partial}{\partial z} \left(\lambda \frac{\partial T_g}{\partial z} \right) - u_0 C_t \tilde{C}_p \frac{\partial T_g}{\partial z} + \varepsilon_b R_g T_g \frac{\partial C_t}{\partial t} - (1 - \varepsilon_b) a_p h_f (T_g - T_p) - \frac{4 h_w}{D_w} (T_g - T_w) - \varepsilon_b C_t \tilde{C}_v \frac{\partial T_g}{\partial t} = 0 \quad (6)$$

where \tilde{C}_v and \tilde{C}_p are the gas molar specific heats at constant volume and pressure, respectively, R_g is the ideal gas constant, D_w is the internal wall diameter, λ is the axial heat dispersion coefficient, h_f and h_w are the film heat transfer coefficients between the gas phase and the particle, and the gas phase and the wall. T_g , T_p and T_w are the gas, particle, and wall temperatures, respectively.

The energy balance of heat transfer through the wall, neglecting the axial heat conduction on the column wall:

$$\rho_w \tilde{C}_{pw} \frac{\partial T_w}{\partial t} = \alpha_w h_w (T_s - T_w) - \alpha_w U (T_w - T_\infty) \quad (7)$$

where T_∞ is the external temperature, ρ_w is the wall density, $\tilde{C}_{p,w}$ is the wall specific heat per mass unit, U is the overall heat transfer coefficient α_w is the wall thickness.

The energy balance to the solid phase:

$$(1 - \varepsilon_b) \left[\varepsilon_p \sum_{i=1}^n \bar{C}_{pi} \tilde{C}_{vi} + \rho_p \sum_{i=1}^n \bar{q}_i \tilde{C}_{v,ads,i} + \rho_p \tilde{C}_{p,s} \right] \frac{\partial T_p}{\partial t} - \left(\lambda_{solid} \frac{\partial^2 T_p}{\partial z^2} \right) = (1 - \varepsilon_b) \left(\varepsilon_p R_g T_p \frac{\partial C_t}{\partial t} \right) + \rho_b \left[\sum_{i=1}^n (-\Delta H_i) \frac{\partial \bar{q}_i}{\partial t} \right] + (1 - \varepsilon_b) a_p h_f (T_g - T_p) - \frac{4}{d_w} h_w (T_p - T_w) + \frac{I^2 \rho(T)}{[(1 - \varepsilon_b) \pi R_w^2 L]^2} \theta \quad (8)$$

where $\tilde{C}_{v,ads,i}$ is the molar specific heat of component i in the adsorbed phase at constant volume, $\tilde{C}_{p,s}$ is the adsorbent specific heat per mass unit, λ_{solid} is the axial heat conduction

in the solid phase and $(-\Delta H_i)$ is the heat of adsorption of component i . I is the electric current passing through the bed, θ is the coefficient of the effective energy employed in the heating of the adsorbent (Ribeiro et al., 2012) and ρ is the electric resistivity of the packed bed, which is temperature-dependent. This temperature dependence was evaluated experimentally.

The multicomponent extension of the Dual-Site Langmuir model:

$$q_i = q_{sat,1,i} \frac{b_{1,i} P_i}{1 + \sum_{j=1}^n b_{1,j} P_j} + q_{sat,2,i} \frac{b_{2,i} P_i}{1 + \sum_{j=1}^n b_{2,j} P_j} \quad (9)$$

$$b_{k,i} = b_{\infty,k,i} \exp\left(\frac{-\Delta H_{k,i}}{R_g T}\right) \quad (10)$$

where $q_{sat,1,i}$ and $q_{sat,2,i}$ are the adsorption saturation capacities of each site for component i , $b_{\infty,k,i}$ is the adsorption constant at infinite temperature and $(-\Delta H_{k,i})$ is the heat of adsorption for each site k (1 and 2) and each component i , and T is the system temperature. The isotherms parameters are given in Table 1.

Table 1. Dual-Site Langmuir model parameters for CO₂ and N₂ adsorption equilibrium on 100%AC, 70%AC-30%13X and 50%AC-50%13X pellets

	$q_{sat,1}$ (mol/kg)	$q_{sat,2}$ (mol/kg)	$b_{0,1}$ (bar ⁻¹) $\times 10^5$	$b_{0,2}$ (bar ⁻¹) $\times 10^5$	$(-\Delta H)_1$ (kJ/mol)	$(-\Delta H)_2$ (kJ/mol)
100%AC						
CO ₂	13.463	2.322	4.14	1.37	19.7	27.1
N ₂	0.581	1.406	1.74	20.9	7.9	18.5
70%AC-30%13X						
CO ₂	6.489	0.742	2.64	0.176	24.2	40.8
N ₂	2.379	1.239	34.8	5.02	13.1	20.2
50%AC-50%13X						
CO ₂	2.026	4.535	2.95	0.642	34.1	28.4
N ₂	3.617	0.866	18.6	353	14.5	8.9

The ESA cycle considered contains four steps. The boundary conditions for the ESA steps employed in the simulations are given in Table 2.

Table 2. Model boundary conditions

Feed	
$z = 0, \text{ INLET}$ $u_{0inlet} y_{inlet} C_{inlet,T}$ $= u_0 y_{0,i} C_i - \varepsilon_b D_{ax} C_T \frac{\partial y_i}{\partial z}$ $u_{0inlet} C_{inlet,T} = u_0 C_T$ $u_{0inlet} y_{inlet} C_{inlet,T} C_p T_{inlet}$ $= u_0 C_T C_p T_g - \lambda \frac{\partial T_g}{\partial z}$	$z = L, \text{ OUTLET}$ $\frac{\partial C_i}{\partial z} = 0$ $P = P_{outlet}$ $\frac{\partial T_g}{\partial z} = 0$
Closed Column Electrification	
$z = 0, \text{ INLET}$ $\frac{\partial C_i}{\partial z} = 0$ $\frac{\partial T_g}{\partial z} = 0$ $u_0 = 0$	$z = L, \text{ OUTLET}$ $\frac{\partial C_i}{\partial z} = 0$ $\frac{\partial T_g}{\partial z} = 0$ $u_0 = 0$

Counter-current Depressurization

$z = 0, \text{ OUTLET}$ $\frac{\partial C_i}{\partial z} = 0$ $\frac{\partial T_g}{\partial z} = 0$ $P = P_{high}$ $+ (P_{purge} - P_{high})(1 - \exp(-\beta t))$	$z = L$ $\frac{\partial C_{g,i}}{\partial z} = 0$ $\frac{\partial T_g}{\partial z} = 0$ $u_0 = 0$
---	--

Purge

$z = 0, \text{ OUTLET}$ $\frac{\partial C_i}{\partial z} = 0$ $P = P_{purge} + (P_{feed} - P_{purge})(1 - \exp(-\beta t))$ $\frac{\partial T_g}{\partial z} = 0$	$z = L, \text{ INLET}$ $u_{0inlet} y_{inlet} C_{inlet,T}$ $= u_0 y_{0,i} C_i - \varepsilon_b D_{ax} C_T \frac{\partial y_i}{\partial z}$ $u_{0inlet} C_{inlet,T} = u_0 C_T$ $u_{0inlet} y_{inlet} C_{inlet,T} C_p T_{inlet}$ $= u_0 C_T C_p T_g - \lambda \frac{\partial T_g}{\partial z}$
---	---

The pellets CO₂/N₂ selectivity was estimated, considering multicomponent adsorption of a 20%/80% CO₂/N₂ mixture at 1.50 bar and 298 K, and the following order was obtained: 50%AC-50%13X (41.9) > 70%AC-30%13X (24.6) > 100%AC (12.2). Then, in terms of selectivity, 50%AC-50%13X is the best option. The heat conductivity of the material is a crucial property for application in an ESA process. The main obstacle identified in this process for CO₂ capture is the lack of an adsorbent material that combines good adsorption properties and electric properties needed for the Joule effect. Considering these two properties in the three materials, according to Regufe et al. (2020), 50%AC-50%13X could be the most appropriate option. However, the referred work did not evaluate the material composition influence while considering the unit optimal conditions. Therefore, the present work will use the material composition as a decision variable, concomitantly with the duration of each step of the ESA unit: Feed (t_{feed}), Closed Column Electrification (t_{elec}); Counter-current Depressurization (t_{oelec}); Purge (t_{purge}). The optimization problem will have a focus on the maximization of the unit productivity while minimizing its energy consumption, considering the CO₂ purity as a constraint. To represent the material composition in its explicit form as a decision variable, three phenomenological models were used, each containing different adsorption equilibrium isotherms. Thus, it was possible to build a database where the material composition represents each model that generated the dataset. Therefore, the deep learning model can use this feature directly as model input.

3. DEEP LEARNING MODELS IDENTIFICATION

The DNN model identification is an essential step of the method proposed here. Thus, a series of steps are proposed to be carefully followed to produce a reliable and precise model. The methodology here employed can be listed as:

- Design of experiments and build of training database;
- Definition of predictor and its hyperparameter;
- DNN training tuning;

- DNN structure optimization and final model validation.

3.1 Design of experiments and build of the training database

The Latin Hypercube Sampling (LHS) technique is a useful tool for the design of experiments, which is usually applied in the literature for AI models identification (Helton and Davis, 2003; Sant Anna et al., 2017; Oliveira et al., 2020). The LHS is based on the near-random generation of the conditions using a cumulative probability density function and correlation analysis.

Therefore, the LHS was used to design the experiments to be done in the virtual plant. A total of 200 sets of operating conditions were designed, which were applied in each of the three models. Each set of operating conditions was composed of the decision variables, which in the present case was the material composition, the amount of activated carbon in the material, and the duration of the steps (t_{feed} , t_{celec} , t_{oelec} and t_{purge}). These operating conditions were then applied in the virtual plant, which was executed for 30 cycles to lead the process to its new steady state. Therefore, a total of 18000 data points were generated, containing the process dynamics evaluation for the target performance parameters: CO₂ purity, ESA productivity, and energy consumption. This data set was divided into two parts, one with 80% of the data for the training procedure and another with the remaining data for the validation procedure.

3.2 Definition of the predictor structure and its hyperparameter

The definition of the predictor is an essential preliminary step. This will impact how the data will be structured to be presented to the nonlinear function approximator. A proper selection of the predictor (data structure) will produce a concise and reliable model. As in the present study, the goal is to build a recurrent deep network; the most adequate choice is the Nonlinear Output Error (NOE) predictor (Oliveira et al., 2020), as referred to in the literature. The NOE structure can be represented as:

$$\begin{aligned} p(t) \\ = F[p(t-1), u(t-d), \dots, u(t-d-n_b+1)] \quad (11) \\ \hat{y}(t) = p(t) + v(t) \end{aligned}$$

where u is the input, d is the input delay, $v(t)$ is the white noise, n_b is the embedded dimension, the number of past values to represent the system dynamics, \hat{y} is the model prediction.

As it is possible to see from equation 11, the NOE has two parameters that need to be defined. The delay d , for the present case, was considered equal to zero, as the first principle model here employed does not comprise the dynamic dead-times. On the other hand, the embedded dimension n_b needs to be computed. In this case, the Lipschitz coefficients were used, as proposed in the literature (He and Asada, 1993; Wang et al., 2003; Oliveira et al., 2020). After computing the Lipschitz coefficients, it was possible to verify that the optimal embedded dimension was equal to 3.

3.3 Deep learning training tuning, optimization and final models validation

With the generated database, it was possible to proceed with the training of the DNN models. As previously mentioned, it was chosen a MISO approach, as it is sought to produce models with reliable precision for each performance parameter. For each DNN model, the tuning of the training optimization method was done. Table 3 presents optimal tuning parameters for all models after performing a sensitivity analysis of each parameter.

Table 3. Training optimization parameters

OPTIMIZATION TECHNIQUE	ADAM
EPOCHS	300
LEARNING RATE	0.001
BATCH SIZE	128
EARLY STOP, VALIDATION PATIENCE	30

After tuning the optimization strategy, the training can proceed concomitantly with the definition of the optimal structure of the DNN models. Therefore, the following points were evaluated: units type [gated recurrent unit (GRU), long short-term memory (LSTM)]; optimal number of hidden layers [1-5]; optimal number of neurons in each hidden layer [1-120]; and the optimal activation functions [relu, tangh, linear]. The DNNs were trained within the ranges of each structural parameter. For each trained model, the validation performance was evaluated, and the optimal one corresponds to the smallest validation MAE (mean absolute error). Table 4 presents the optimal structures and MAE values for each structure. For all the DNNs, a GRU unit was identified as the optimal strategy. However, the LSTM performance was close to the GRU, and the difference between the methods should be deeper evaluated in the future.

Table 4. Optimal DNN structures (optimal number of layers, type of layer, neurons and activation function).

PURITY MODEL, MAE = 1.29		
LAYER	ACTIVATION	NEURONS
GRU	RELU	100
GRU	RELU	80
GRU	RELU	80
DENSE	TANH	60
DENSE	LINEAR	1
PRODUCTIVITY MODEL, MAE = 0.14		
LAYER	ACTIVATION	NEURONS
GRU	RELU	110
GRU	RELU	80
DENSE	TANH	60
DENSE	LINEAR	1
ENERGY CONSUMPTION MODEL MAE = 4.87		
LAYER	ACTIVATION	NEURONS
GRU	RELU	80
GRU	RELU	100
GRU	RELU	80
DENSE	TANH	40
DENSE	LINEAR	1

*RELU - RECTIFIED LINEAR FUNCTION
 *TANH - HYPERBOLIC TANGENT FUNCTION

The predictions of the validated models are presented in Fig. 1; few disturbances are presented in the figure for a clean visualization of the system dynamics. However, the validation set contained 3600 cycles. In the figure, it is possible to see that the models provide a good approximation of both the dynamic and cyclic state of the ESA unit.

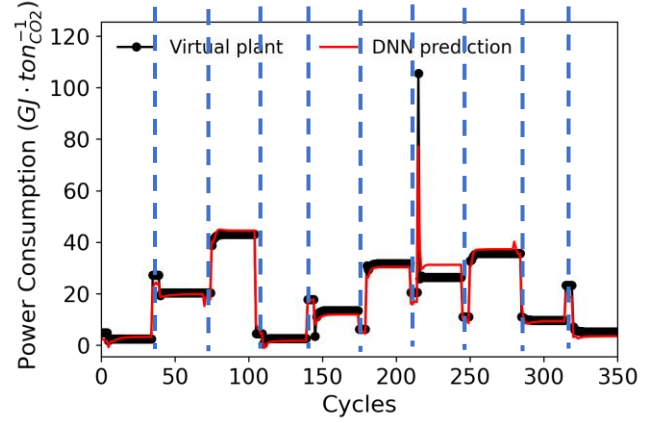
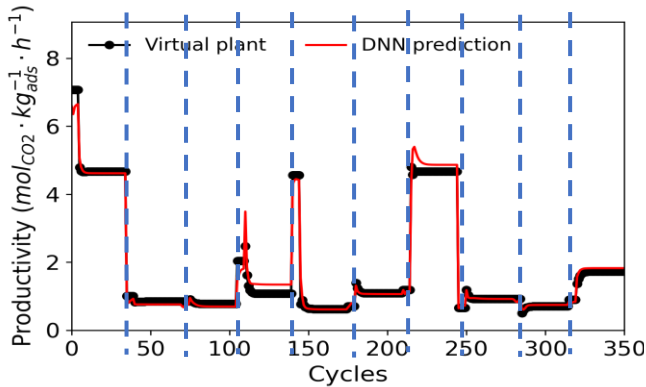
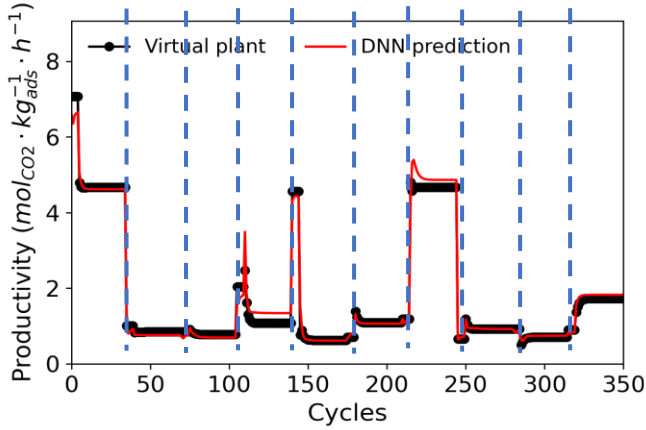
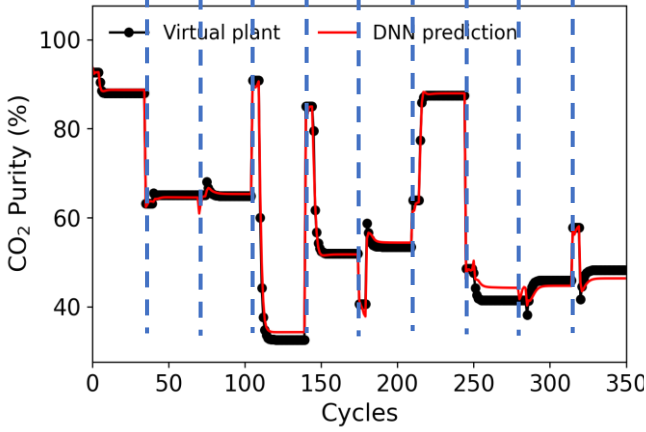


Fig.1. DNN models validation; dashed vertical lines represent disturbances moment.

4. OPTIMIZATION PROBLEM

Finally, making use of the identified models, it is possible to evaluate the optimal material composition while simultaneously considering the process optimization. It is necessary to design an objective function that comprises the desirable goals while embodying the material properties in its set of decision variables.

$$\min_D V_k \quad (12)$$

$$V_k = \delta_E \cdot E_{cons} - \delta_p \cdot Pr_{CO_2} \quad (12a)$$

$$s.t. \quad (12b)$$

$$Pur_{CO_2} > 0.95 \quad (12b)$$

$$D \in [D_{min}, D_{max}] \quad (12c)$$

where δ_E and δ_p are the weighting factors, and D is the set of decision variables, which should obey a compact and convex set of constraints, corresponding to these variables bounds. Therefore, as it is performed a dynamic simulation these variables are computed along the time, forming a set of path constraints. Finally, the CO_2 purity should follow an end-point constraint evaluated at the unit cyclic steady state.

The optimization problem presented in equation (12) can be read as find the set of process operating conditions (t_k) and the material composition (y_{AC}) that will simultaneously minimize the energy consumption and maximize CO_2 productivity while keeping the CO_2 purity above 96% and respecting the decision variables bounds.

The range of the material composition was defined by the synthesized materials in the experimental studies performed by Regufe et al. (2020), as described in section 2.1. The particle swarm optimization, a meta-heuristic approach, was employed to solve the optimization. A total of 200 particles and 200 iterations were used.

Table 5 summarizes the optimization results obtained after following the proposed methodology. It is possible to note that the optimal set of decision variable was provided, in which the optimal material composition is 50% of activated carbon and 50% of zeolite 13X. Furthermore, it is possible to see that the method was able to find an optimal condition for the process performance parameters while respecting the purity constraint.

Table 5. Optimization results, decision variables and optimal performance parameters

OPTIMAL SET OF DECISION VARIABLES				
t_{feed}	t_{celec}	t_{oelec}	t_{purge}	Composition
245	277	3	14	50% AC
PERFORMANCE INDICATORS				
PURITY (%)	Productivity ($mol_{CO_2} \cdot kg_{ads}^{-1} \cdot h^{-1}$)	ENERGY CONSUMPTION ($Gj \cdot ton_{CO_2}^{-1}$)		
99.6	9.6	0.18		

Fig.2 presents the evolution of the objective function along with the optimization procedure; it is possible to see in this figure that after 80 iterations, the algorithm is already very close to the minimum of the objective function. Each optimization iteration takes only a few seconds to be executed.

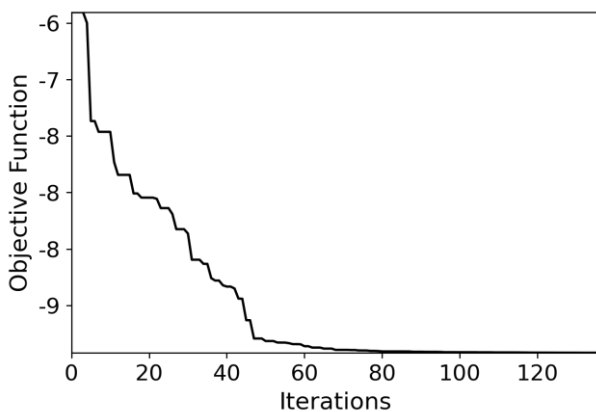


Fig.2. Objective function evolution during the meta-heuristic optimization.

5. CONCLUSIONS

In this work, a novel methodology was presented to perform material screening and process optimization. The method is based on the Deep Neural Network model to identify reliable and computationally fast models. As an optimization strategy, it was employed a meta-heuristic algorithm. An objective function was proposed in order to accommodate the materials screening and process operating conditions as optimization variables to address a conflicting goal, optimize productivity and energy consumption. As a case study, it was presented the CO₂ capture using an Electric Swing Adsorption process at bench-scale. The results demonstrated that the methodology could efficiently define the optimal conditions while providing optimal material composition. Furthermore, the optimization based on DNN models reduces significantly the computational effort, while using a first principles models it would be required several days to obtain an optimization result, through the DNN based method this result can be obtained in few minutes (5 minutes in the present case). Thus, it is possible to conclude that the method can be applied in real-time scenarios where process reconfiguration is necessary.

REFERENCES

- He, X., Asada, H., 1993. A New Method for Identifying Orders of Input-Output Models for Nonlinear Dynamic Systems. In: 1993 American Control Conference. IEEE, pp. 2520–2523.
- Helton, J.C., Davis, F.J., 2003. Latin hypercube sampling and the propagation of uncertainty in analyses of complex systems. *Reliab. Eng. Syst. Saf.* 81, 23–69.
- Nogueira, I., Fontes, C., Sartori, I., Pontes, K., Embiruçu, M., 2017. A model-based approach to quality monitoring of a polymerization process without online measurement of product specifications. *Comput. Ind. Eng.* 106.
- Nogueira, I.B.R., Ribeiro, A.M., Requião, R., Pontes, K. V., Koivisto, H., Rodrigues, A.E., Loureiro, J.M., 2018. A quasi-virtual online analyser based on an artificial neural networks and offline measurements to predict purities of raffinate / extract in simulated moving bed processes. *Appl. Soft Comput. J.* 67, 29–47.
- Oliveira, L.M.C., Koivisto, H., Iwakiri, I.G.I., Loureiro, J.M., Ribeiro, A.M., Nogueira, I.B.R., 2020. Modelling of a pressure swing adsorption unit by deep learning and artificial intelligence tools. *Chem. Eng. Sci.* 224.
- Ongari, D., Talirz, L., Smit, B., 2020. Too many materials and too many applications, an experimental problem waiting for a computational solution.
- Rajagopalan, A.K., Avila, A.M., Rajendran, A., 2016. Do adsorbent screening metrics predict process performance? A process optimisation based study for post-combustion capture of CO₂. *Int. J. Greenh. Gas Control* 46, 76–85.
- Regufe, M.J., Ferreira, A.F.P., Loureiro, J.M., Rodrigues, A., Ribeiro, A.M., 2020. Development of Hybrid Materials with Activated Carbon and Zeolite 13X for CO₂Capture from Flue Gases by Electric Swing Adsorption. *Ind. Eng. Chem. Res.* 59, 12197–12211.
- Ribeiro, R.P.P.L., Grande, C.A., Rodrigues, A.E., 2012. Electrothermal performance of an activated carbon honeycomb monolith. *Chem. Eng. Res. Des.* 90, 2013–2022.
- Sant Anna, H.R., Barreto, A.G., Tavares, F.W., de Souza, M.B., 2017. Machine learning model and optimization of a PSA unit for methane-nitrogen separation. *Comput. Chem. Eng.* 104, 377–391.
- Wang, C., Klatt, K., D, G., Engell, S., Hanisch, F., 2003. Neural network-based identification of SMB chromatographic processes. *Control Eng. Pract.* 11, 949–959.

ACKNOWLEDGMENTS

This work was financially supported by: EDUFI Fellowships program, Base Funding - UIDB/50020/2020 of the Associate Laboratory LSRE-LCM - funded by national funds through FCT/MCTES (PIDDAC); FCT – Fundação para a Ciência e Tecnologia under CEEC Institucional prog, Brazilian research agency FAPESB under grant BOL0731/2020.